An Engineering Approach of an X-Ray Car Crash Under Reverse Small Overlap Configuration

Y. Leost[1], A. Nakata[2], P. Bösl[1], I. Butz[1], T. Soot[1], M. Kurfiß[1], S. Moser[1], F. Kase[2], T. Hashimoto[2], S. Shibata[2]

[1] *Fraunhofer Institute for High-Speed Dynamics, Ernst-Mach-Institut, EMI, Am Klingelberg, 79588 Efringen-Kirchen, Germany*

[2] *Honda R&D Co., Ltd., Tochigi, Japan*

Abstract

During a crash event, conventional optical measuring systems provide information about the deformation of parts that are directly visible. The new measuring method called X-Ray Car Crash (XCC) developed at Fraunhofer EMI allows accessing the crash kinematic of specific parts inside the vehicle. This method provides precious information that is currently not accessible in a crash test and allows for better comparison with FEM simulations. The present paper describes a preliminary study performed in collaboration with Honda R&D Co., Ltd. The load case under consideration is a reverse variant of the IIHS Small Overlap with integrated X-Ray technology.

Fraunhofer EMI Research Crash Center aims at developing new measurement methods to investigate non-standard high-speed dynamics safety issues. Most of these specific requests are coming from car manufacturers. In order to achieve maximum test reproducibility and simplify boundary conditions, the facility is equipped with a propelled sled system on rails. Thus, it enables to perform impactor to vehicle scenarios with moving barriers up to 3000 kg by 22 m/s.

The standard Small Overlap at 64 km/h belongs to the vehicle to barrier scenario and requires some preliminary computations to adapt it for the EMI Crash test facility. Special consideration was given to energy balance in order to determine the right barrier velocity and mass to achieve a similar intrusion in the car to in the standard configuration.

Numerical simulations were required at each step to meet the different challenges of this study. This paper describes first the numerical assessment of the validity of the reverse scenario. FEM simulations were then used extensively for developing a special moving barrier presenting maximal structural robustness, well-balanced dynamic behavior and allowing on-sled measurement technics and braking system. Then, LS-DYNA® simulations provided necessary data to perform ray tracing simulations and thus finding the right placement for X-ray source and X-ray detector. Finally, numerical simulations played an important role for an enhanced test setup, by finding the best balance between appropriate mechanical robustness of supporting structures (so called Pit-cover) and low X-ray attenuation.

Keyword: Small Overlap, X-Ray, Reverse Crash Test, HyperG, LS-DYNA

Introduction

The overall objective of the project was to perform an X-ray car crash based on the small overlap test at 64 km/h [1] at the EMI crash-test facility, as shown in Figure 1. This test aims at observing the deformation of specific parts inside the car during the crash.

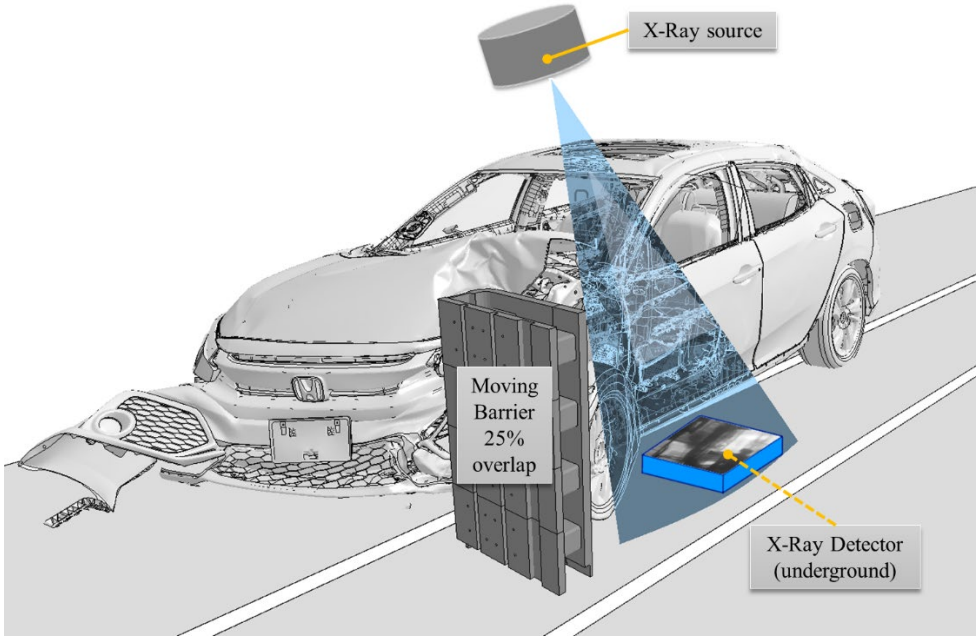

Figure 1: Overview of the reverse Small Overlap test configuration with X-Ray device.

Simulation tools had to provide all information and digital material necessary to perform the full vehicle test. This included the definition of the instrumental needs as well as the design and optimization of the test setup. Simulation activities covered many different aspects of the project, among which:

- The car deformation and the internal energy have to be similar in the normal and the reverse scenario. Thus, the project aimed at investigating the influence of a reverse crash configuration.
- No critical plastic failure should occur neither on the sled/rails nor on the barrier. Special consideration was given to critical parts such as force sensors and guidance bearings for which a maximal load limit was determined.
- Development of an appropriate moving barrier with integrated load cells. Optimization of the overall impactor mass that should remain under 3000 kg to follow facility operating instructions [2]. Optimization of the crash stability by reducing the impactor pitch and yaw in the crash event.
- Determine car trajectory to optimize the X-ray system placement and guaranty facility integrity.

Finite Element Development

Investigations of reverse crash effects

An investigation of reverse crash effects was necessary to develop a test setup, where the resulting energy, force and deformation of the car are similar to the standard IIHS Small Overlap. This chapter contains an analytical discussion based on the energy balance in a similar way as presented in the Equivalent Speed Energy study [3] and a validation of this model using simplified FEM-simulations.

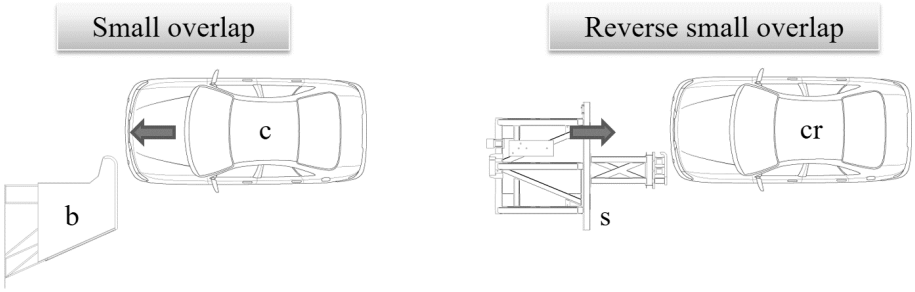

Figure 2: Comparison between standard crash scenario (left) and reverse (right).

In the normal scenario, the car is moving and the barrier is fixed ("infinite" mass object). In the reverse scenario, the barrier is moving and the car is not fixed, see Figure 2. It is assumed that both objects will have a non-zero kinetic energy immediately after impact and that the impactor does not deform. By neglecting the friction of the wheels directly after the impact, it is possible to link the parameters of the normal scenario with those of the reverse scenario. See chapter "Nomenclature" for the definitions of variables.

Neglecting the external friction forces at the impact, the conservation of total momentum gives

$$m_{cr}u_{cr} + m_s u_s = m_{cr}v_{cr} + m_s v_s \quad (1)$$

Eq. (1) is then simplified as $m_{cr} = m_c$ which is known from the original scenario, and $u_{cr} = 0$.

Neglecting yaw energy, the energy balance can be expressed as

$$\frac{1}{2}m_{cr}u_{cr}^2 + \frac{1}{2}m_s u_s^2 = \frac{1}{2}m_{cr}v_{cr}^2 + \frac{1}{2}m_s v_s^2 + E_d \quad (2)$$

Assuming that both objects are moving with the same velocity after impact,
Eq. (1) yields:

$$m_s u_s = (m_c + m_s)\, v_s \quad (3)$$

Eq. (2) yields:

$$m_s u_s^2 = (m_c + m_s)\, v_s^2 + 2\, E_d \quad (4)$$

Thus, replacing the sled velocity after impact in Eq. (4) using Eq. (3) gives a relationship between sled mass and sled velocity for a given kinetic energy in the original scenario:

$$m_s = \frac{2\,E_d\,m_c}{m_c u_s^2 - 2\,E_d} \tag{5}$$

For computational efficiency, the FEM model of the Ford Fiesta was used to estimate the error caused by the simplifying assumptions underlying Eq. (5). This model was developed by the National Crash Analysis Center (NCAC) and contains about 20.000 elements. Both normal overlap test and reverse test were simulated, see Figure 3. The barrier was simplified as a flat barrier, which is a valid assumption in the context of this study. The computation of the standard scenario at 64 km/h with the Fiesta model (905 kg) yields a car deformation energy of 120 kJ. This deformation energy was set as a goal for the reverse scenario, which was computed with two different car masses: a first variant with 905 kg, and a second variant with 1500 kg. For the second variant, virtual mass was added proportionally on the heaviest car PIDs. The basic idea to reduce the sled mass in the reverse scenario is to increase the car mass which leads to an increase of the reaction forces against the impact and thus to a higher deformation energy.

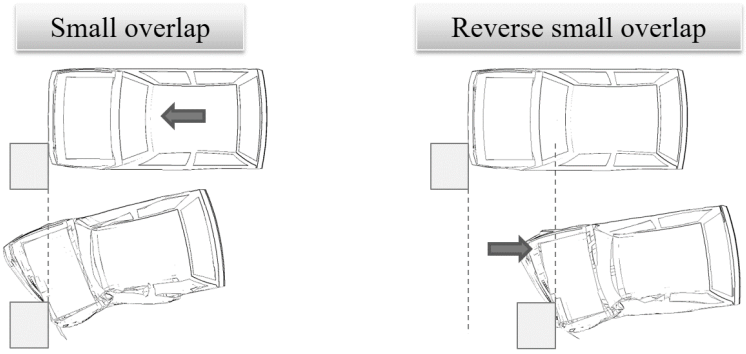

Figure 3: Standard scenario with moving car against fixed barrier (left), and reverse scenario with moving barrier (right).

An iterative simulation process was performed with the reverse scenario by varying the barrier mass to achieve the same amount of internal energy as in the normal scenario. Results are presented in Figure 4.

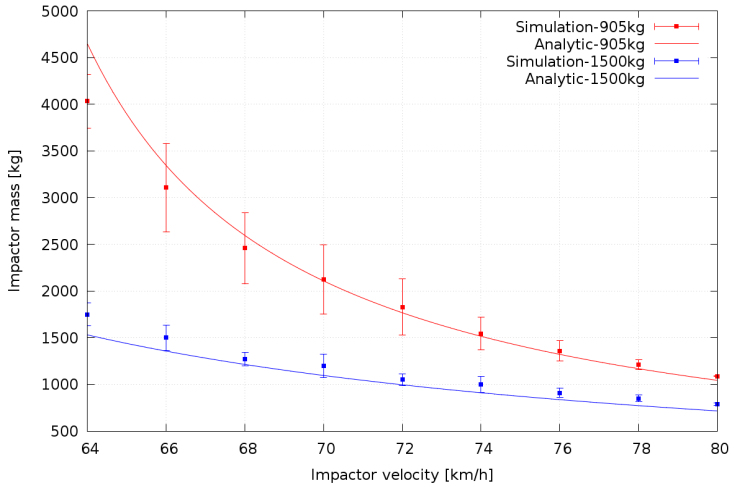

Figure 4: Comparison of the analytical model with simulation results for Ford Fiesta 905 kg and 1500 kg resulting in a 120 kJ deformation energy.

Additional simulations were performed at a given velocity in order to estimate the relation between deformation energy and car mass. These simulations revealed an overall trend with some scatters. Thus, using impactor mass vs. internal energy plots, an estimation of the error was done for each velocity. The resulting dispersion was higher for the lighter car variant (red) than for the heavier one (blue). Some discrepancies between the simulations and the analytical model were still observable. This could be explained by the simplifying assumptions of the analytical model where for example friction at the ground and yaw energy are neglected. From this analysis, it can be concluded, that an increase of the car mass by 66% allows for a reduction of the impactor mass by 57% at 64 km/h. Therefore, it was possible to reduce the impactor mass and stay within the facility operating range.

FEM sled and barrier models

A realistic sled FEM-model with 460.000 elements was developed and validated at Fraunhofer EMI. This LS-DYNA model has an average element size of 15 mm, except for guidance parts (Figure 5) where the average element size is 6 mm. The default LS-DYNA version used for now is the mpp971_r7_1_2.

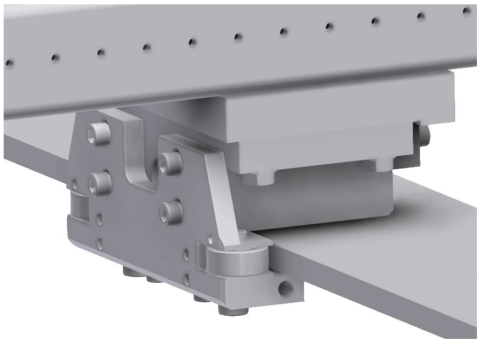

Figure 5: Overview of the guidance system with rails and side bearings.

Simulation activities helped developing safer test conditions. Due to the offset configuration with high kinetic energy and resulting lateral forces, the test configuration was suspected to be challenging for the guidance system. Thus, critical parts like bearings, shafts and guidance brackets had to be modeled accurately.

During the project, quasi-static compression tests were performed on the side bearings and shaft in order to identify their loading limits, see Figure 6. The force-displacement curve inflexion at 215 kN is due to the shaft bending. It is challenging to estimate precisely a load limit, up to which the bearing remains functional. Therefore, for simulation purpose, the limit for the side bearings was set to 160 kN (80% of the maximal load observed in experiment). The detailed modeling of the shaft and bearing from Figure 6 was then used to develop a realistic simplified model for the sled simulation.

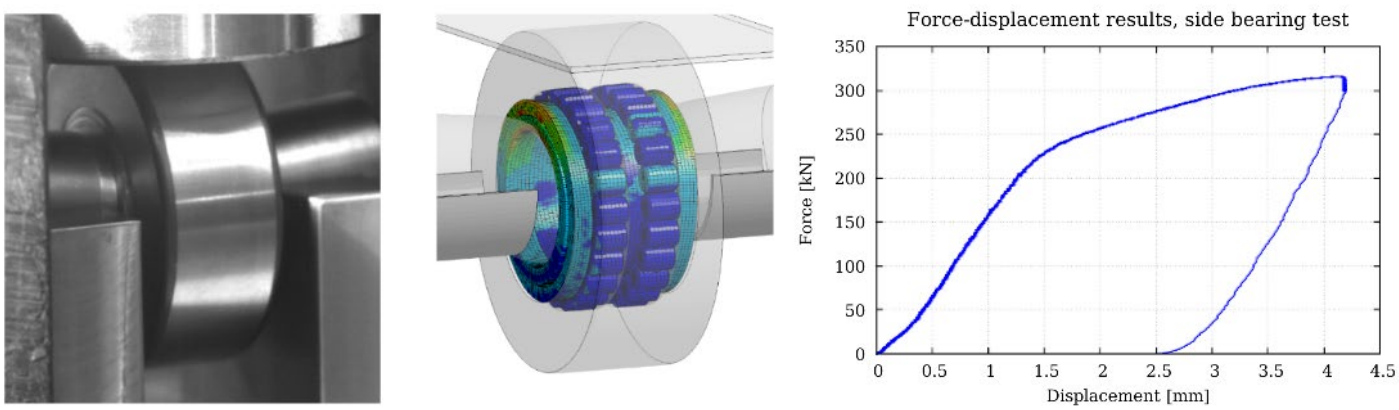

Figure 6: Quasi-static compression test on side bearings and simulation results with von Mises stress contour.

The original small overlap barrier is extremely heavy and not intended to be movable. Thus, the barrier was redesigned, keeping the same radius at the edge but reducing the dimensions and the overall number of load cells. After the simplification, only 8 load cells were still considered in the barrier, which allowed for a comparison of the forces in experiment with those from FEM simulations. As the barrier should allow for 1200 mm intrusion, no supporting structure was permitted on the left side. An iterative development of the barrier was performed by varying the number of reinforcements, their position and the overall mass. The final barrier design is presented in Figure 7.

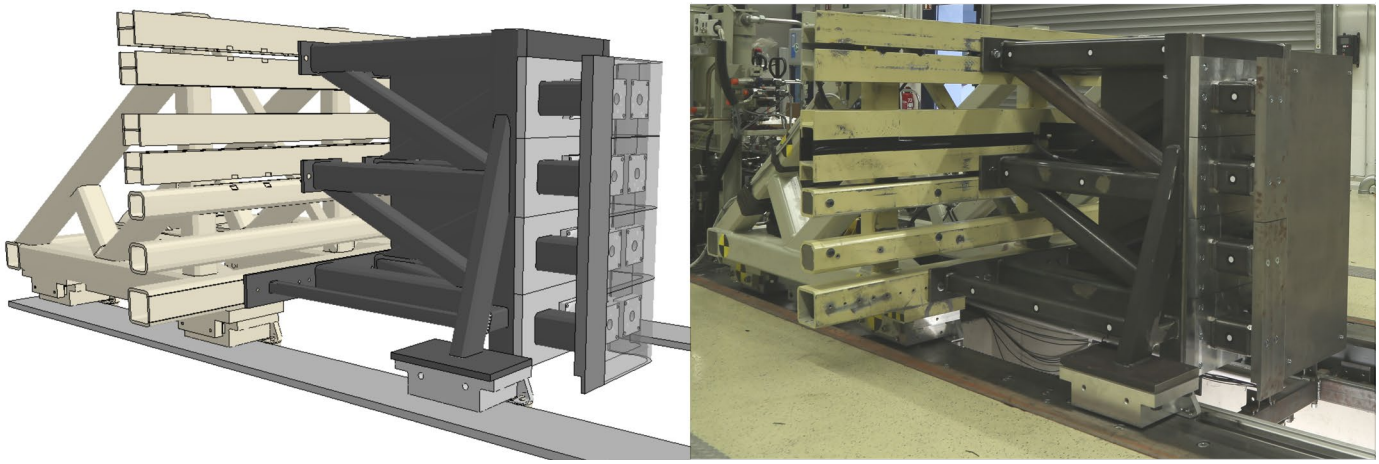

Figure 7: FEM impactor model with sled and barrier final design (left) and its construction (right). Load cells are visible on the FE model by transparency.

X-Ray Prediction Method

Description of the Method

Using high-speed X-ray diagnostics, the deformation processes of certain parts of interest can be observed during the crash. To do so, during the crash experiment, several X-ray images were taken of the moving car using pulsed X-ray sources to avoid blurring due to the fast motion of the car. The experimental X-ray setup requires detailed planning prior to the experiment, which was performed using the X-ray prediction method described below.

Virtual X-ray projections of the part of interest were generated to help ensure its visibility on the acquired X-ray images during the crash experiment. Computation of these virtual X-ray images was based on a raytracing approach. Here, the geometry of the entire car as well as material information was taken from the FEM model. Using FEM data as input for a raytracing approach is a challenge, because it contains volumetric elements as well as shell elements. For this application, shell elements were approximatively transformed to volumetric elements by assuming an element thickness drawn from the FEM input files.
Using the planned experimental setup of X-ray source and detector, X-ray absorption was approximated as following: X-rays were assumed to travel on a straight line between source and respective detector pixel, and scattering was neglected. Using the geometry and material information of the car, path lengths of each X-ray through the different materials were computed. The intensity of X-ray radiation decays exponentially over the length of material passed scaled with an energy dependent, material specific attenuation coefficient (Beer-Lambert-Law). Here, as a first-order approximation, the attenuation coefficient was assumed to be proportional to material density, where its energy dependency was neglected. Additionally to accounting for the Beer-Lambert-Law, the simulated X-ray intensities were scaled using contrast and brightness settings, which can be modified manually.
Based on these assumptions, X-ray absorption was estimated for each detector pixel, generating a virtual X-ray projection. Note, that the purpose of this X-ray simulation is not the generation of physically correct simulated X-ray projections. Instead, it was used for the visualization of the car geometries to be imaged in order to enable optimization of the experimental X-ray geometry and therefore maximize visibility of the part of interest during the crash.

Results and Discussion

Test setup

The test setup is shown in detail in Figure 8.

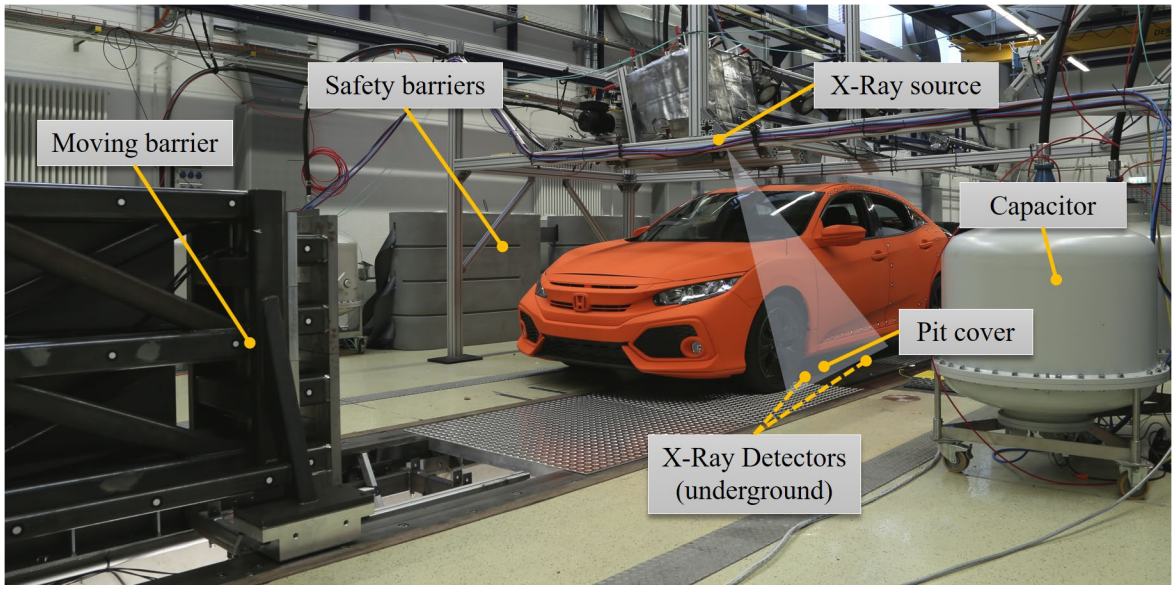

Figure 8: Test setup.

An important task here was the development of a suitable pit cover. The pit cover has to provide enough bending resistance while at the same time offer low photon attenuation to provide a higher X-ray image quality on the detector. Different materials and thicknesses were considered based on theoretical knowledge about mechanical stiffness and photon attenuation. Knowing that the flexural rigidity D of a plate is given by [4]

$$D = \frac{Et^3}{12(1-\nu^2)} \tag{6}$$

and that a narrow beam of mono-energetic photons with an incident intensity I_o, penetrating a layer of material with mass thickness t and density ρ, emerges with intensity I given by the exponential attenuation law (Beer-Lambert) [5]

$$I/I_0 = e^{-\frac{\mu}{\rho}t} \tag{7}$$

Assuming that the attenuation of X-rays in the air is negligible, it is possible to plot the bending stiffness against the attenuation rate of the medium used. Results are presented in Figure 9.

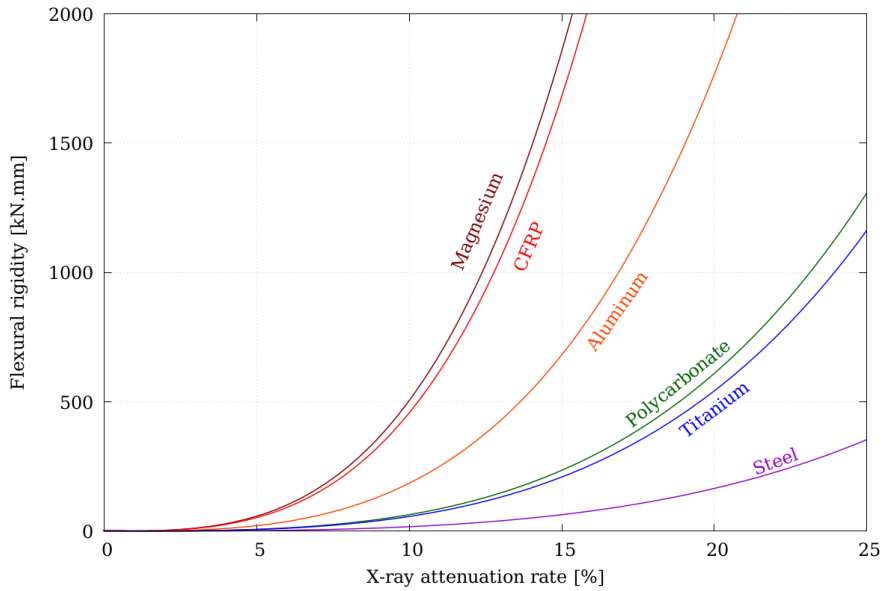

Figure 9: Flexural rigidity against X-ray attenuation rate for different materials.

For a given flexural rigidity, the choice of the medium is crucial to avoid too much attenuation of X-rays. Thus, aluminum plate with a thickness of 7 mm was chosen for practical reasons. Plate deflection and bold stresses were checked after having estimated the tire load on the ground with basis of full car simulations, as shown in Figure 10.

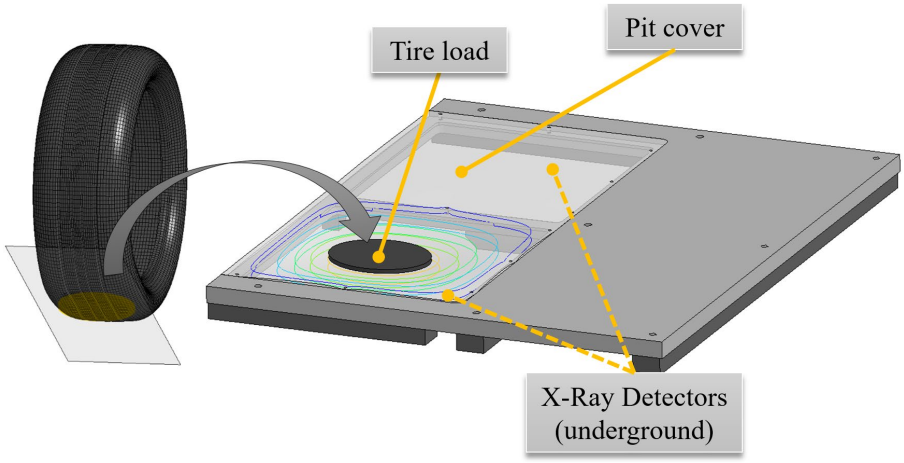

Figure 10: Simulation of pit cover loading with consideration to maximal deflection.

Simulation results with Customer model

The investigations of inverse crash effects allowed for considerable reduction of the domain of input parameters. Even though it is theoretically possible to match the 64 km/h standard scenario with a 80 km/h reverse impact velocity, it is likely to trigger different deformation modes in the structures due do inertia and strain rate dependency of the materials. For this reason, solutions with a velocity close to the velocity in the standard scenario are preferred. Thus, the domain of input parameters was restrained to:

$$\begin{cases} 64\ km/h \ \leq\ v_{Impactor} \leq 68\ km/h \\ 1500\ kg \leq\ m_{Car} \leq 1750\ kg \\ 2200\ kg \ \leq\ m_{Impactor} \leq 2600\ kg \end{cases}$$

Based on this domain of input parameters, a Design of Experiment approach was used. For each set of input parameters, the intrusion of several points in the region of interest inside the car was compared to the simulation of standard scenario and reverse scenario. An error index was calculated based on the root mean square error. Results are presented in Figure 11.

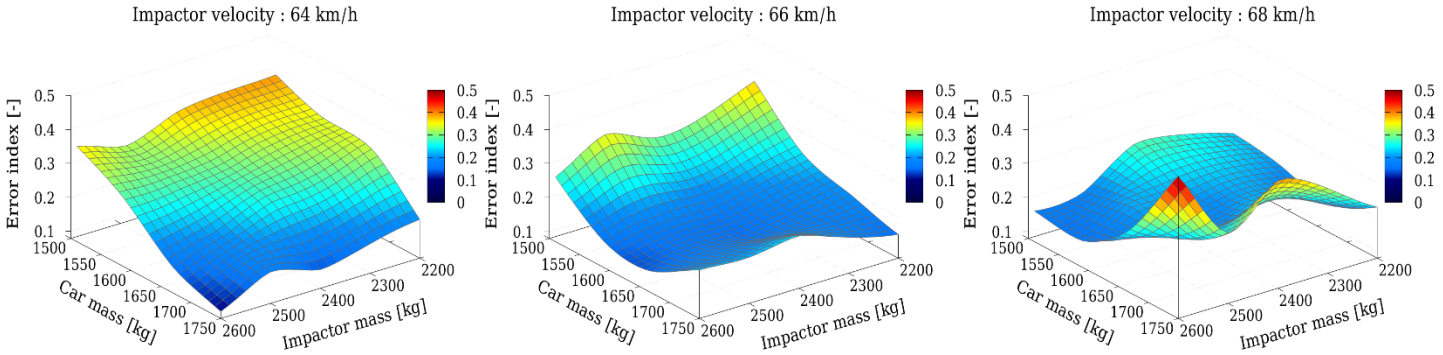

Figure 11: Design of Experiments with customer FEM car model.
Error response surface against Car and Impactor masses.

From the response surface, the best inverse scenario with lowest error index could be identified. This scenario has the same velocity as the standard one, with a car mass of 1750 kg and an impactor mass of 2600 kg. Simulation analysis of this case showed no plastic strain on the impactor, no critical loads on the bearings (Figure 12), but also forces under the limit of 500 kN on the Kistler load cells.

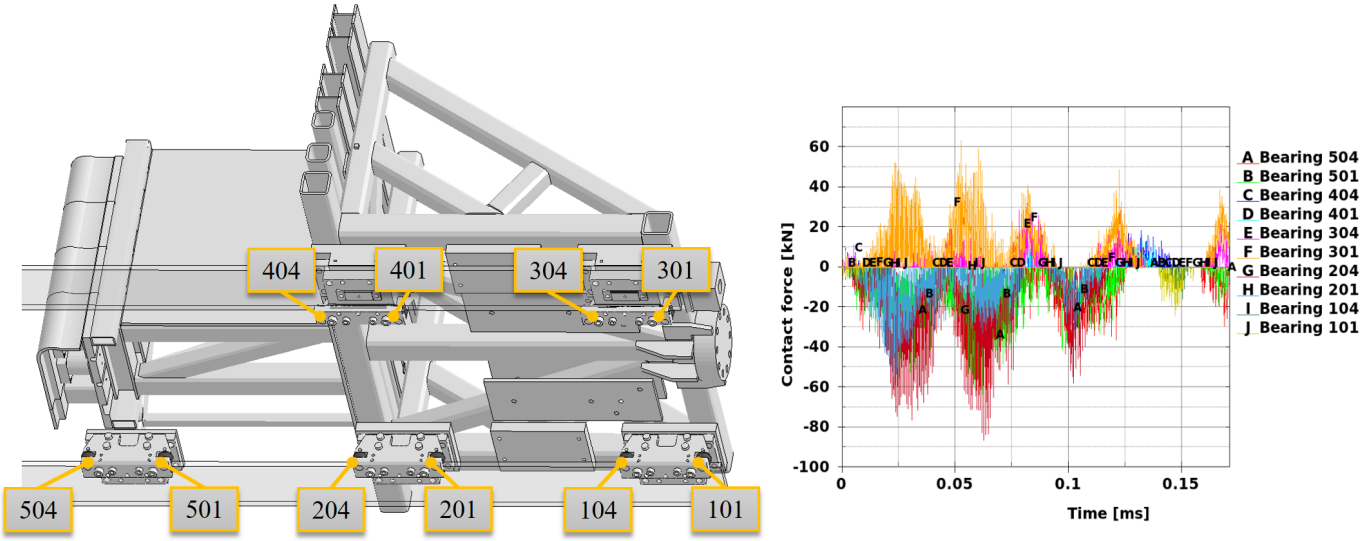

Figure 12: Forces acting on side bearings during the crash event.

Results of X-Ray pre-test simulation

As a first step, the experimental X-ray setup was designed. To do so, the spatial 3D coordinates of relevant nodes on the part of interest were taken from the FEM simulation data for the relevant time steps and their trajectory was visualized. An example of the trajectory and feature projection is given for three features in Figure 13. Note, that in this case the nodes to be tracked were pre-defined positions on the part of interest, which do not produce distinctive features on the X-ray image. Therefore, in the experiment, X-ray markers were attached to the chassis in the area of interest at the pre-defined positions, which enable recognition of the relevant nodes on the X-ray image. For a better identification of the small X-ray markers on the X-ray images, they were made of dense materials like for instance tungsten.
The X-ray geometry was optimized so that the relevant nodes were situated within the field of view (framed in orange in Figure 13) for all imaging time points. Additionally, when planning the imaging setup, experimental constraints had to be considered, e.g. the detectors had to be placed within the pit and the sources had to be positioned high enough so that they cannot be hit by the sled or car. In several iterations, the setup was optimized under these boundary conditions.

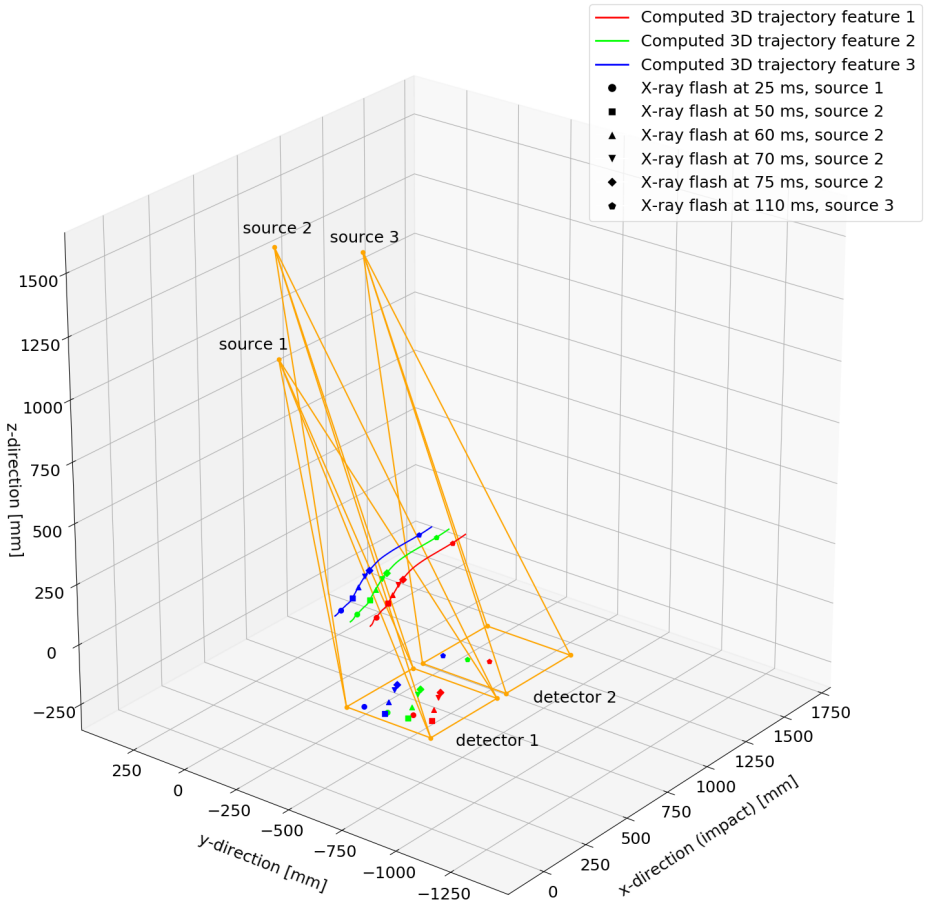

Figure 13: 3D plot of planned X-ray geometry and trajectories of some relevant object features.

Figure 14 shows the resulting images obtained with the proposed setup via X-ray simulation: Images were taken using three sources and two detectors to be able to cover the trajectories of the relevant nodes on the part of interest.

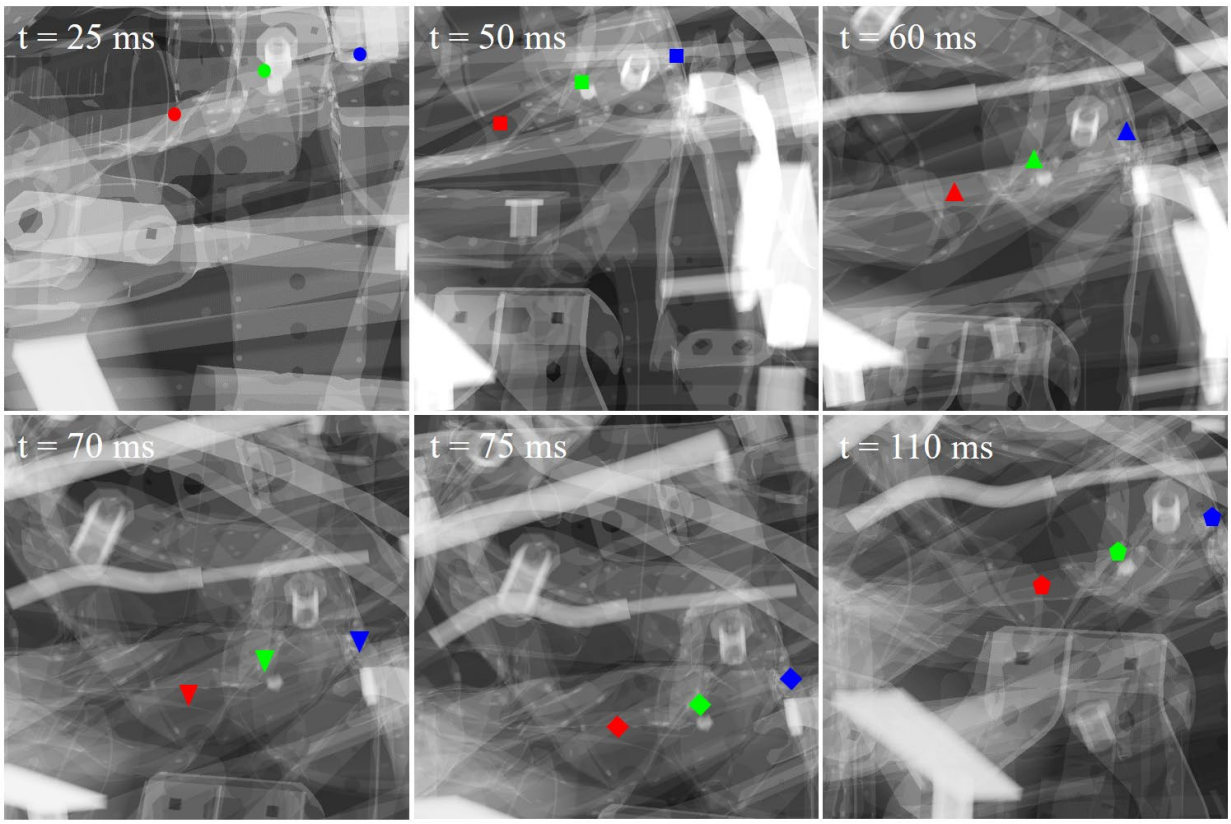

Figure 14: Time series of virtual X-ray projections using the proposed imaging geometry. Exemplary predicted marker positions are highlighted in color.

To provide visibility of most features on the detector images, raytracing X-Ray projections were computed for each planned imaging time point using the proposed imaging geometry. A time series of the resulting X-ray projections showing the projected positions of the three exemplary nodes are displayed in Figure 14. As the X-ray markers are not included in the FEM model, they are not visible in the X-ray images. However, by projecting the positions of the relevant nodes, the predicted location of the marker can be highlighted.
It has to be noted, that deviations between simulated and experimentally acquired X-ray projections are to be expected due to the simplifying assumptions underlying the X-ray simulation as well as due to deviations between the FEM model and the real car crash experiment. However, the simulated images based on the FEM model of the car crash allow the conclusion that the plurality of relevant nodes can be expected to be visible on all acquired X-ray images.

Summary and next steps

FEM simulations were used in this study to find the right parameter set for reverse crash test, to develop the test setup, to help ensure facility safety and to investigate the right placement for X-ray sources and detectors. The test setup is currently under construction and the experiment will take place during the next few weeks. This study proved the feasibility and the benefit of an X-ray car crash as the numerical results were very promising. In addition, new tools and methods were developed for an X-ray car crash.
Fraunhofer EMI has already invested in a linear particle accelerator (Linac) to continue developing the X-ray car crash methodology. Linacs are capable of producing a nearly continuous stream of X-ray pulses, which will be a considerable advantage in the future, as the number of X-ray images during the crash will be shot at a frame rate up to 1000 hertz. The first successful demonstration of an X-ray video with a Linac was performed by Fraunhofer EMI and shows the running engine of a Simson moped with a frame rate of 1000 hertz. [6]

Nomenclature

m_c : Vehicle mass in normal scenario
m_{cr} : Vehicle mass in reverse scenario
m_s : Impactor mass in reverse scenario
u_c : Vehicle initial velocity in normal scenario
u_{cr} : Vehicle initial velocity in reverse scenario
u_s : Sled initial velocity in reverse scenario
v_{cr} : Vehicle velocity in reverse scenario after impact
v_s : Sled velocity in reverse scenario after impact
E_d : Vehicle deformation energy. Should be the same in both scenarios
E : Young modulus
t : Elastic thickness
ν : Poisson's ratio
ρ : Density
μ : Attenuation coefficient

References

[1] https://www.iihs.org/ratings/about-our-tests/test-protocols-and-technical-information, Small overlap frontal testing, Test protocol Version VI (July 2017).
[2] https://www.instron.de/de-de/products/testing-systems/crash-simulation/hyperg.
[3] F. A. Berg et Al., Implications of Velocity Change Delta-V and Energy Equivalent Speed EES for Injury Mechanism Assessment in Various Collision Configurations. Dekra Automobil AG and University of Zürich (ETH).
[4] L.D. Landau, E.M. Lifshitz (1986). Theory of Elasticity. Vol. 7 (3rd ed.). Butterworth-Heinemann. p. 42. ISBN 978-0-7506-2633-0.
[5] Creagh, D.C. and Hubbell, J.H. (1992), X-Ray Absorption (or Attenuation) Coefficients, Sec. 4.2.4. in International Tables for Crystallography, Vol. C, A.J.C. Wilson, ed. (Kluwer Academic Publishers, Dordrecht), 189-206.
[6] https://www.emi.fraunhofer.de/en/business-units/automotive/research/x-ray-diagnostics-in-crash-tests-picks-up-speed.html